AIAA JOURNAL
Vol. 34, No. 6, June 1996

Investigation of Large-Scale Structures in Supersonic Planar Base Flows

K. M. Smith* and J. C. Dutton†
University of Illinois at Urbana–Champaign, Urbana, Illinois 61801

Time-resolved, planar imaging was employed to study the spatial organization of large-scale structures within the shear layers, at reattachment, and in the wake region of a supersonic base flow. Side and end views were obtained at several streamwise locations to characterize the evolution and three-dimensionality of the large-scale motions. From statistically significant ensembles, spatial correlation fields were computed to quantify the mean size, eccentricity, and orientation of the large structures. Visualizations confirm that large-scale turbulent structures exist at all stations in the shear layers and interact vigorously with the recirculation region. Mach and/or shock waves are frequently seen emanating from within the shear layer, which may be indicative of eddy shocklet formation. The embedded turbulent structures are elliptical in shape and usually appear inclined to the mean flow direction. A distinct flattening and tilting in the streamwise direction occur as the coherent eddies negotiate shear layer formation, recompression, and reattachment processes. Spatial statistics indicate that the structures have a streamwise and spanwise spatial extent on the order of the local shear layer thickness. Examinations of spatial correlation fields suggest that the embedded structures are thoroughly three dimensional at all streamwise stations. The structures exhibit a slightly stronger organization in the spanwise direction during the initial region of the shear layer; however, near recompression, a transition occurs in which the streamwise coherency of the structures becomes dominant. Furthermore, the structures appear to degrade in their spatial organization during the recompression and reattachment processes.

Introduction

EFFORTS to understand and to predict the complex interaction processes in the near wake of a supersonic base flowfield have been under way since the advent of long-range missiles in the 1940s and continue to the present time.[1] Initial efforts in supersonic base flow research were motivated by a desire to improve the drag profiles of projectiles, missiles, and airfoils. Recent applications have included other practical applications such as chemical lasers, supersonic exhaust nozzles, and supersonic combustors. The near-wake region of a supersonic base flow persists as a formidable research challenge because of its inherent complexity: large flow gradients in thin shear layers, expansion waves, shock waves, large streamline curvature, compressibility, shear layer impingement, and the effects of turbulence.

Figure 1 presents a schematic of a planar supersonic base flow along with a graphical description of the imaging locations used in this study (discussed later). The approach boundary layers separate from the base corners and undergo a vigorous expansion to form the free shear layers. These newly formed shear layers initially encounter a region of zero pressure gradient mixing, followed by a region of adverse pressure gradient mixing. The two shear layers eventually impinge at reattachment and subsequently accelerate to form the trailing wake. For a supersonic vehicle, the shear layers border a strong recirculation region immediately behind the base. The interaction of these shear layers with the recirculation zone, specifically mass entrainment and its effect on the mean base pressure, is an important component of the overall drag mechanisms on the vehicle.

Recently, compressible shear layers have been the subject of considerable research effort, primarily because of their importance in propulsion systems for hypersonic aircraft. Planar visualizations have provided concrete evidence that large-scale structures are present in high-speed compressible shear layers and that their mean structure is significantly affected by the overall level of compressibility.[2–4] Structures with well-formed cores and interconnecting braids are clearly seen for low-to-moderate compressibility; however, at higher levels of compressibility, the structures appear to be more filament-like with a decreased coherence in both the spanwise and streamwise directions. Furthermore, at high compressibility, the structures tend to become more elliptical in shape and skew obliquely to the mean flow. It has been proposed that the structural degeneration observed at high compressibility can be attributed to the dominance of three-dimensional instability modes.[5–7]

Laser Doppler velocimetry studies of the supersonic planar near-wake region[8,9] have suggested the existence of large-scale structures within the shear layers. Although point-by-point velocity measurements provide valuable mean and turbulence statistics, they are limited in obtaining a thorough understanding of large-scale structures' characteristics since only the influence of these structures can be recorded. Individual structures themselves cannot be captured in the raw data.

The present study is believed to be the first to employ planar imaging techniques for the near-wake interaction of two dissimilar supersonic streams separated by a finite thickness splitter plate. The

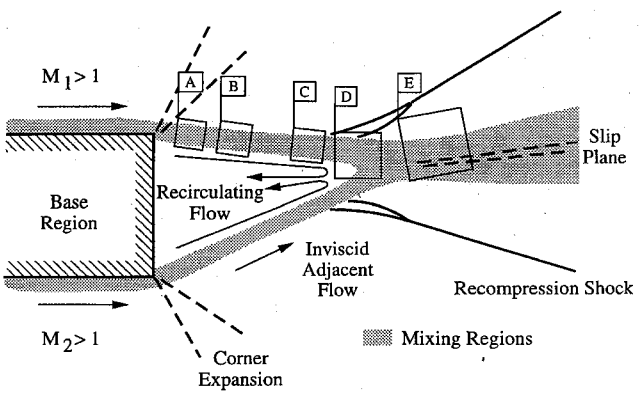

Fig. 1 Description of fields of view used in this study and flow processes for the separation of two supersonic streams past a finite thickness base (adapted from Ref. 1).

Presented as Paper 95-2251 at the AIAA 26th Fluid Dynamics Conference, San Diego, CA, June 19–22, 1995; received July 28, 1995; revision received Feb. 5, 1996; accepted for publication Feb. 26, 1996.

*Graduate Research Assistant, Department of Mechanical and Industrial Engineering, 1206 West Green Street. Student Member AIAA.

†Professor, Department of Mechanical and Industrial Engineering, 1206 West Green Street. Associate Fellow AIAA.

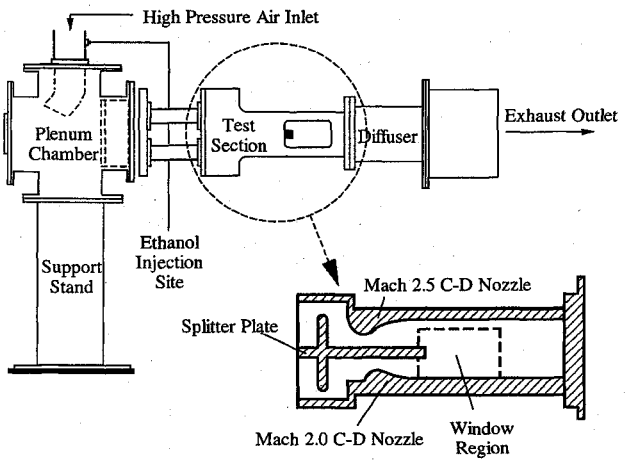

Fig. 2 Physical arrangement and test section internals of planar base flow wind tunnel.

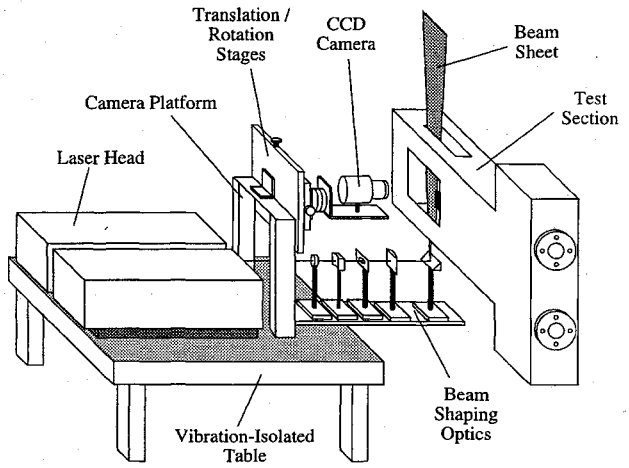

Fig. 3 Mie scattering image acquisition system.

initial development of the free shear layer closely approximates that of the traditional zero pressure gradient, zero streamline curvature mixing layer. Downstream of the zero pressure gradient mixing region, the flowfield depicted in Fig. 1 permits the effects of streamline curvature, recompression, and reattachment on the spatial evolution of coherent motions to be characterized. The qualitative images and quantitative measurements presented here help clarify the influence of the large-scale structures on the shear layers and recirculation region, as well as their contribution to wake development.

Facility and Equipment

The high-speed flow experiments of this study were performed in the Gas Dynamics Laboratory at the University of Illinois at Urbana–Champaign using a blowdown-type wind tunnel. Figure 2 is a schematic diagram of the test facility. Compressed air is supplied to the plenum chamber through a series of dryers and filters to ensure that it is dry and free of sizable naturally occurring contaminants. Immediately upstream of the plenum chamber, liquid ethanol is introduced into the carrier air through an atomizing nozzle that produces a polydisperse spray with a median volume diameter of approximately 100 μm. This location provides sufficient residence time for the ethanol to thoroughly evaporate before reaching the test section. A steady tunnel stagnation pressure is maintained through the use of a control valve that receives its command input from a proportional-integral-derivative-type controller operating with a stagnation pressure feedback loop. Nominal stagnation conditions for both streams are $P_0 = 503 \pm 3$ kPa (absolute) and $T_0 = 300 \pm 2$ K. The high-pressure air leaves the stagnation chamber through a flow conditioning module consisting of metallic honeycomb and screens. The flow path is then divided into two separate lines, each supplying its own respective nozzle block. The turning sections and rapid accelerations within the nozzles are responsible for reducing the influence of any residual freestream turbulence. Each stream accelerates through its converging-diverging nozzle to supersonic velocity, negotiates the interaction region behind the base, and exits the test section via a constant-area diffuser and silencer ductwork.

The planar base flow test section produces a Mach 2.5 upper stream and a Mach 2.0 lower stream (with intentional boundary-layer thickness mismatches) that both undergo geometric separation past a thick splitter plate (25 mm in height). The overall dimensions of the test section are 100 mm in height and 50 mm in width. The details of the design and construction of the test section are described by Amatucci.[1] The separation, shear layer development, recompression, reattachment, and wake formation take place in full view of the side windows. To provide optical access for the interrogating laser sheet, the floor and ceiling of the test section were modified by inserting flush-mounted slot windows.

Experimental Diagnostics

The primary diagnostic used in this study was Mie scattering. Implementation of the Mie scattering technique closely follows the passive scalar method described by Clemens and Mungal.[10] As described earlier, liquid ethanol is atomized into the carrier air where it completely evaporates before reaching the test section. The expansion to supersonic conditions promotes a catastrophic collapse of the ethanol's supersaturated state, resulting in an extremely fine condensation fog. The tracer droplets are formed immediately downstream of the nozzle throat and are carried throughout the freestream where they grow only as a result of coagulation. The ethanol droplets are expected to have a Gaussian size distribution with diameter in the range of 0.01–0.1 μm and with a number density on the order of 10^{12} per cubic centimeter.[4,10,11] For the present investigation, a representative Stokes number, defined as the ratio of particle response time to the large eddy rollover time, is 0.06, which indicates that the droplets should faithfully mark the flowfield.[12]

The image acquisition hardware is illustrated in Fig. 3. The Mie scattering study makes use of a high-power pulsed laser for the illumination of the condensed ethanol. The Nd:YAG laser is equipped with a frequency doubling crystal to provide a nominal pulse energy of 550 mJ per pulse at a wavelength of 532 nm. Each laser pulse has a temporal width of 6–8 ns that is sufficiently short to freeze the particle motion. The laser output is formed into a planar sheet through the use of spherical and cylindrical lenses. The resulting beam sheet has a waist thickness of approximately 250 μm (based on Gaussian optics calculations and physical measurements) and an adjustable width of 75–125 mm. For the side views, a 14-bit high-resolution unintensified charge-coupled device (CCD) camera was used to record the scattered light. The end views were obtained using an 8-bit intensified CCD camera, which allowed for a greater depth of field. All images were collected through standard photographic lenses and subsequently stored for postprocessing.

Results and Discussion

The upper half of Fig. 1, which is drawn to scale, illustrates the location and designation of each field of view in this study. Both side-view and end-view images were collected at each of these locations. Although visualizations were performed along both the upper and lower shear layers, only instantaneous images from the upper shear layer survey will be presented here because of space limitations. A detailed comparison of the top and bottom shear layers, including the influence of the strength of the base corner expansion, will be the focus of a future paper. Imaging locations near the base were selected based on consideration of the pressure gradient environment. Positions A and B are located in the initial formation region of the developing shear layer where there is no pressure gradient. Position C is centered in the adverse pressure gradient, i.e., recompression, region before reattachment. Images at these three streamwise stations allow an examination of the effect of pressure gradient on the structural characteristics. Position D is located at the mean reattachment point. Finally, position E is located in the trailing wake. For the side-view images, the camera was inclined relative to the tunnel floor to be aligned with the mean flow direction of the shear

Table 1 Imaging locations and flowfield parameters

Imaging position	Distance from base corner along shear layer, mm	Field-of-view inclination,[a] deg	Convective Mach number, M_c	Shear layer width, δ_{local}, mm
A	7.5	-10.7 ± 0.2	1.27	$1.65 \pm 3\%$
B	15.0	−9.6	1.37	1.95
C	30.0	−5.6	1.25	2.35
D	35.0	0.0	1.12	2.77
E	50.0	11.2	0.74	3.98[b]

[a]Measured with respect to test section floor. Positive angles denote an upward inclination.
[b]An estimate for the half-wake width is used.

layer at each location. In all side-view images to follow, the mean streamwise direction is horizontal in the image from left to right. Table 1 contains the location and inclination (streamwise direction) of the five fields of view. The inclination data, as well as all other quantitative results reported here, have had uncertainty estimates attached to them using the small-sample method[13] with 20:1 odds.

Side-wall pressure surveys[1] indicate that the absolute static pressure is 29.1 and 62.4 kPa at the exits of the Mach 2.5 and 2.0 nozzles, respectively. Both of these streams undergo a centered expansion at the corner to match the base pressure of 13.8 kPa absolute. Using this static pressure information, isentropic calculations predict that the high-speed air bordering the recirculation region for each shear layer is at approximately Mach 3.0 (625 m/s). Earlier LDV data[1] indicate that the reverse flow velocity in the recirculation region can be as high as Mach 0.4 (135 m/s), roughly 22% of the freestream velocity. By using the Mach 3.0 freestream and the local recirculation zone centerline velocity as boundary conditions, the convective Mach number[14,15] M_c for the shear layer at each of the imaging locations has been computed and is presented in Table 1. For position E, the wake centerline velocity was used as the low-speed boundary condition. Before reattachment, M_c is calculated to be fairly constant at about 1.3, which corresponds to a very high degree of compressibility. The overall compressibility of the flow decreases through reattachment and wake formation. The unit Reynolds number along the free shear layer is estimated to be approximately 37×10^6 per meter. Velocity and density ratios along the initial portion of the shear layer are approximately 0.21 and 0.37, respectively.

Parametric studies of ethanol loading indicated that a 0.35% mass fraction produced the optimal fog uniformity for imaging. A simplified analysis of the Rayleigh flow effects as a result of the condensation heat release[16] confirmed that the ethanol did not significantly degrade the operating conditions at the test section. For example, the condensation process was predicted to lower the effective nozzle Mach numbers by less than 1%. Polarization studies revealed that the scattered signal from the ethanol droplets is extremely sensitive to incident polarization (therefore in the Rayleigh scattering regime), suggesting that the particles are much smaller than originally estimated. The actual Stokes number for the flow is most likely considerably lower than the 0.06 value presented earlier.

For the side-view images, the laser sheet was brought into the tunnel as depicted in Fig. 3. To illuminate the flowfield for the end views, the beam sheet was rotated 90 deg by adjusting the cylindrical lenses in the optics train. All images were recorded using a nominal laser pulse energy of 350 mJ at 532 nm. The scattered signal was collected with a Micro-Nikkor 105-mm photographic lens set at $f2.8$ ($f16$ for end views) coupled to a 27.5-mm extension ring. Although the minimum resolvable spatial wavelength in the image plane[17] was approximately two orders of magnitude larger than the representative Kolmogorov scale for the flow, the system has sufficient spatial resolution to capture the dominant large-scale structures of interest.

Typical signal-to-noise ratios, defined here as the mean signal level divided by the detector's noise floor, were roughly 25 for the side views and 17 for the end views. The signal quality for the end views was degraded by the necessity to image at an oblique angle (approximately 40 deg to the flow direction) through the side windows. A simple geometric correction was applied to the raw end-view data to correct for the perspective defect introduced by the oblique view. The raw images were processed to remove laser reflections and camera dark current by subtracting an average background image. Spatial variations in the scattered signal as a result of the laser sheet profile and droplet coagulation were removed by normalizing the instantaneous images by a reference image. The images are rendered using a gray-scale convention, where white is the seeded freestream (high signal) and black is warm recirculation region fluid with no condensation (low signal).

The shear layer width δ_{local} at each location was determined by averaging 512 instantaneous images and locating the top and bottom edges of the shear layer, as defined by 10 and 90% of $(I_{max} - I_{min})$, where I_{max} is the signal intensity in the seeded freestream and I_{min} is the signal intensity in the recirculation region. These shear layer breakpoints are analogous to the 10 and 90% velocity difference points used by Goebel and Dutton[18] for determination of shear layer width from velocity data. Table 1 contains the calculated shear layer widths at each imaging location. In all of the images to be presented, the local shear layer width is indicated in the image margin as a relevant length scale. The placement of δ_{local} in the image margin also indicates the mean transverse location of the shear layer.

Side-View Instantaneous Images

A side-view Mie scattering image of the entire near-wake interaction region is presented in Fig. 4. Although difficult to discern in this low-magnification view, stringy, filament-like structures can be seen projecting into the recirculation region from within the shear layers. Near reattachment, the structures are a distinct feature of the flowfield, and shock patterns are evident in the proximity of these structures. The shocks are discernible because the Mie scattering signal is proportional to the number density of the scattering particles. Fluid that has been compressed by a shock is denser and therefore permits a higher signal to be collected. Although the flow is globally seeded, no condensate is observed in the recirculation zone. The relatively low velocities in the base region correspond to thermodynamic conditions near the stagnation temperature, thereby promoting re-evaporation. The base region provides evidence that re-evaporation of the ethanol is occurring in this flowfield; therefore, special consideration of the thermodynamic conditions throughout the flowfield must be maintained when interpreting the images. A detailed calculation has determined that the flowfield will not support wholesale recondensation of the base region ethanol until well downstream of the observation locations shown in Fig. 1.

The structural characteristics of the large-scale motions observed at positions A and B are qualitatively very similar; therefore, side-view images at position A are not included here because of space limitations. Four Mie scattering images at position B, in the constant pressure shear layer region, are presented in Fig. 5. Although large-scale structures clearly exist at this location, no rounded Brown–Roshko-type rollers[19] are detected, nor are any vortex interactions such as pairing. Similar structures were observed at position A, confirming that large-scale structures are, in fact, present immediately downstream of separation. The structures at both locations do not display the consistency and spatial uniformity observed in supersonic shear layers at lower convective Mach numbers.[2–4,20] Frequently, the shear layer structure appears highly irregular in nature with jagged interfacial features. This breakdown in coherency can be attributed to the increased influence of three-dimensional instability modes at high convective Mach numbers.[7] The dominant spatial organization of the coherent motions seems to be elliptical in shape; however, no distinct recurring pattern is seen. The eddies appear to be inclined toward the streamwise direction, with long filament-like

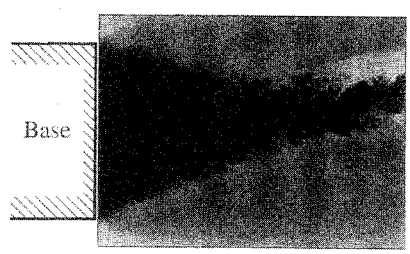

Fig. 4 Mie scattering image of entire near-wake region.

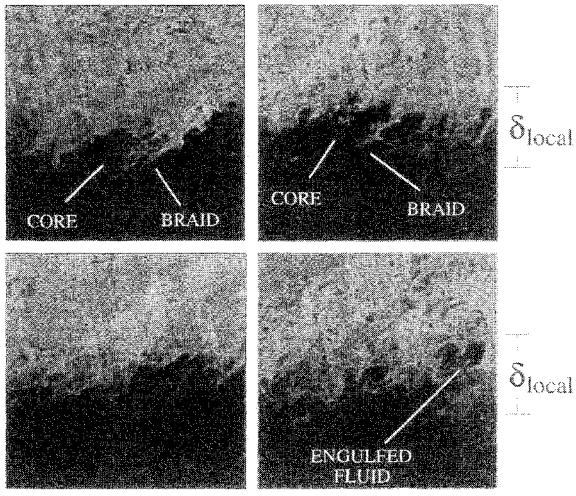

Fig. 5 Side-view Mie scattering images taken at position B (image dimensions are 5.7 × 5.7 mm).

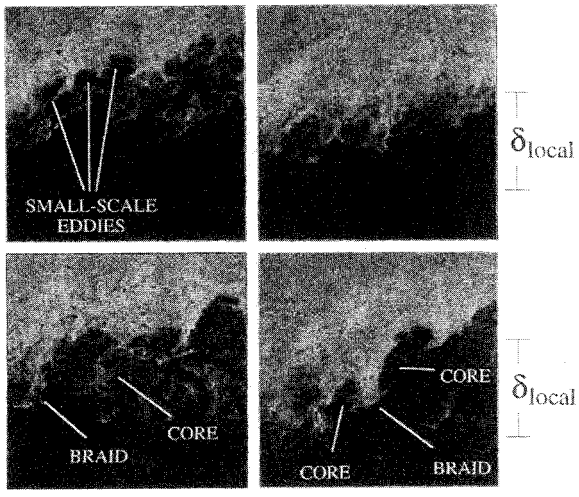

Fig. 6 Side-view Mie scattering images taken at position C (image dimensions are 5.7 × 5.7 mm).

braids connecting the highly strained cores. Although the structures are generally small relative to the base dimension, they are considered large scale in the sense that they possess a spatial extent on the order of the local shear layer thickness. The noticeable nonuniformities in the marked freestream fluid, which appear as dark blobs or streaks, are believed to be the remnants of the boundary layer that have persisted beyond the corner expansion. In the lower right image of Fig. 5, it appears that a parcel of low-speed recirculating fluid has been completely surrounded by freestream fluid because of some type of vortical motion. Entrainment of recirculating fluid into the shear layer by this apparent engulfment process should result in a reduced base pressure as suggested by a simple mass subtraction argument.

Figure 6 illustrates the coherent structures and the accompanying compression waves that form the base of the global recompression shock in the recompression region (position C). These eddies exhibit a greater diversity in size and shape than seen at earlier streamwise stations. For example, the upper right image of Fig. 6 shows a somewhat passive shear layer, devoid of significant spatial organization; however, the lower right image of Fig. 6 illustrates at least two distinct structures and a sharp braid. Examination of Fig. 6 also indicates the presence of small-scale structures residing on large-scale structures. Theoretically, all large-scale structures have attendant small-scale structures residing on them. The resolution capabilities of the current imaging system permit the discernment of small-scale structures only at later stations of the shear layer where they have grown to an appreciable size. In the upper left image in Fig. 6, three

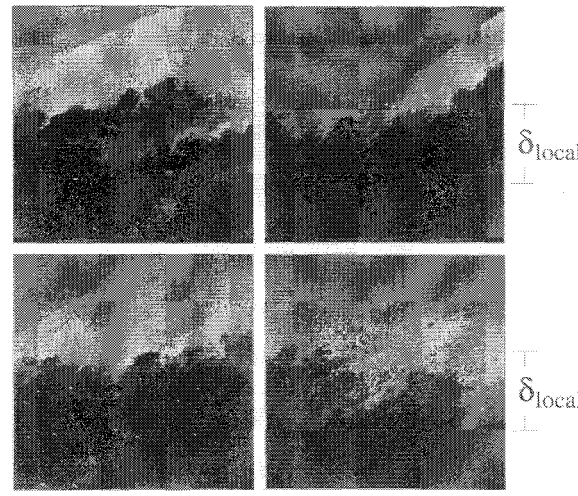

Fig. 7 Side-view Mie scattering images taken at position D (image dimensions are 8.3 × 8.3 mm).

small eddies appear to be residing on a much larger structure. Elliott et al.[21] also observed embedded small-scale structures in supersonic shear layers at $M_c = 0.51$ and 0.86. The shear layer of the current study is seen to pitch (or flap) in the recompression region, with a maximum deviation from its nominal position of approximately one-half δ_{local}. The quality of the freestream condensation fog has also improved relative to that at position B, probably because of the dissipation of the boundary-layer remnants.

Figure 7 presents instantaneous images of the shear layer at reattachment (position D). The large-scale structures observed immediately after separation (positions A and B) and during recompression (position C) have grown to become dominant features of the flowfield. The structures often make deep excursions into the reattachment region, which appears to pulsate as the shear layer pitches up and down. Shock waves emanating from within the shear layer, which apparently form because of the presence (interference) of the large-scale structures with the supersonic outer flow and/or the recompression process at reattachment, usually originate radially on the leeward side of an eddy. It would appear that the shocks in the shear layer are of nonuniform strength: stronger near the structures (where local flow acceleration is most pronounced) and weaker away from the structures (as evidenced by the increasing obliquity to the freestream flow). Whether these shocks are, in fact, actually the eddy shocklets discussed by Dimotakis[22] is inconclusive at the present time. Future efforts will utilize a double-pulsed technique capable of capturing two time-correlated images of the coherent structures. From these data, it will be determined if the shock wave travels with the structure or if the shock is stationary.

Figure 8 presents several images in the trailing wake (position E). A diverse collection of both large-scale and small-scale structures is present. Several examples of shock origination from the eddies are clearly visible, as well as the coalescence of several individual shocks into the bounding recompression shock. The spatial organization of the structures varies from almost strict periodic spacing (upper left) to an apparently random ordering (lower left). The structures appear to be elliptical in nature and inclined appreciably toward the mean flow direction. The small tufts of condensed ethanol near the wake centerline are believed to be fragments of structures that were torn during reattachment. It is also possible that the tufts are evidence of incipient recondensation of base fluid that has been pumped into the wake.

End-View Instantaneous Images

Figure 9 presents end-view images at reattachment (position D). End-view images at positions A, B, C, and E will not be presented here since the broad spectrum of structural sizes, shapes, and spacing seen at all streamwise stations are well represented by the images in Fig. 9. As previously described, the quality and resolution of these images are significantly less than the side-view images because of unavoidable degradations as a result of the oblique viewing angle;

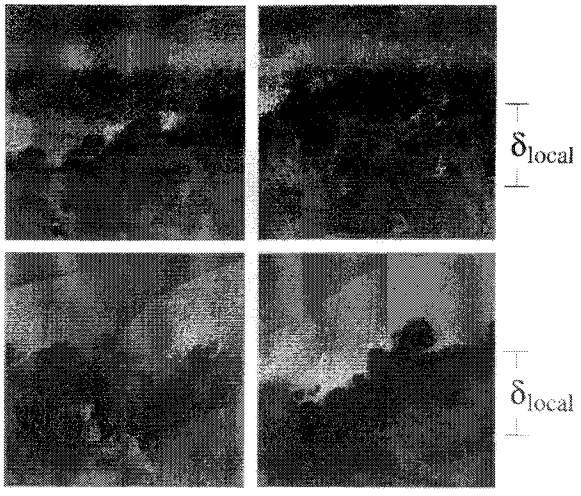

Fig. 8 Side-view Mie scattering images taken at position E (image dimensions are 11.2 × 11.2 mm).

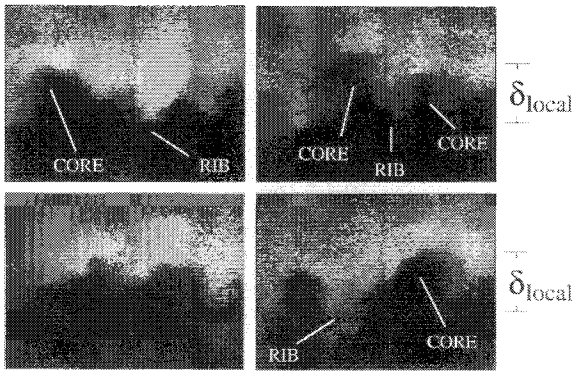

Fig. 9 End-view Mie scattering images taken at position D (image dimensions are 8.3 × 11.1 mm).

however, the structural characteristics in the spanwise-transverse plane are still perceptible. The dominant structural feature appears to be finger-like projections descending from the high-speed side of the shear layer into the recirculation region and vice versa. Clemens and Mungal[2] and Messersmith[4] also saw evidence of similar ejections of fluid into the freestreams for $M_c = 0.79$ and 0.75, respectively. The interface between the marked and unmarked fluid is corrugated, creating troughs of varying depth and width between neighboring projections. It is expected that streamwise vorticity would participate in the entrainment process by convecting recirculation region fluid into these troughs. Clemens and Mungal[23] also found evidence in their plan views of an $M_c = 0.79$ shear layer that pure low-speed fluid was being carried to the center of the shear layer by streamwise vortices. It appears that the structures at reattachment are tilted away from a strictly vertical orientation. This tilting, along with the highly convoluted appearance of the interface, suggests that oblique motions are present. The convective Mach number at reattachment is about 1.12, which is well into the regime where oblique instability modes are expected to be dominant.[7] A common feature of the images in Fig. 9 is the presence of high-intensity regions bordering the cross-stream structures. These high-intensity regions may be indicative of shock waves that are in close proximity to the structures.

Statistical Analysis

The structural diversity of the instantaneous eddies at any given location makes it extremely difficult to quantify the average spatial characteristics of the large-scale structures. To reduce the influence of observer bias in this study, large ensembles of instantaneous images were processed statistically to objectively determine the mean size, shape, and orientation of the coherent motions. Root-mean-square and spatial correlations fields were computed according to the procedure described by Miles and Lempert.[24] A parametric study determined that an ensemble size of 512 images would ensure stable statistical results.

When computing the spatial correlations, it is necessary to prescribe a location in the image about which the spatial lags will be performed. To reduce the subjectivity of the reference point selection, five reference points within the shear layer were used. These reference points were located on the central column of the image and corresponded to transverse locations of $\eta = -0.25, -0.125, 0.0, 0.125$, and 0.25, where η is a nondimensional transverse coordinate defined from the average image as $\eta = (y - y_0)/\delta_{local}$ and y_0 is the center of the shear layer, specified as the location with an intensity that is 50% of $(I_{max} - I_{min})$. The five individual correlation fields were computed and then averaged. For each of the correlation fields to be presented, the contour lines are in even increments of 0.1 about the central peak, which has a value of unity by definition. The 0.5 contour level is used for the determination of structure size and inclination. Contour levels below 0.5 are not included for clarity.

Side-View Spatial Correlations

Figure 10 presents five spatial correlation fields, corresponding to locations A–E in Fig. 1, computed from the ensembles of side-view images. Note that all correlation fields in Fig. 10 are oriented such that the local mean streamwise direction is horizontal from left to right. Immediately following separation (position A), the average structure appears to be elliptical in shape with an inclination of the structure's major axis toward the streamwise direction. At position B, which is in the constant pressure region, the structures seem to evolve by growing in dimension only, without appreciable departure from the qualitative features observed at position A. At position C, the correlation field exhibits a noticeable tilting toward the streamwise direction and an increase in eccentricity, which is defined as unity minus the ratio of the minor axis dimension to the major axis dimension. The tilting and flattening of the structures continue through reattachment (position D), where the

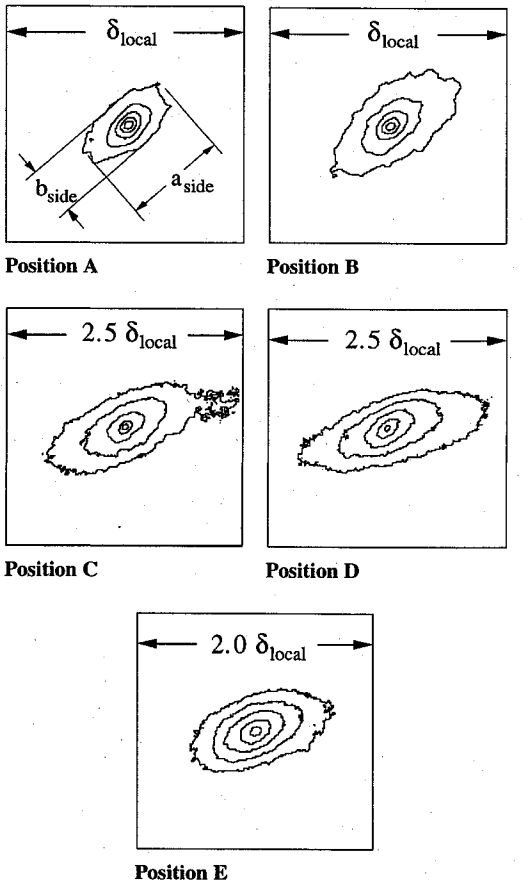

Fig. 10 Side-view spatial correlation fields; the contours are in intervals of 0.1, and the outermost contour represents the 0.5 level.

Table 2 Side-view correlation results

Position	Major axis dimension, a_{side}, mm	Nondimensional structure size,[a] a_{side}/δ_{local}	Eccentricity,[a] $\varepsilon = 1 - (b_{side}/a_{side})$	Structure angle,[b] deg
A	0.71 ± 0.05	0.43 ± 0.04	0.50 ± 0.05	41.2 ± 2.0
B	1.24	0.64	0.54	40.1
C	3.96	1.69	0.61	24.6
D	5.56	2.01	0.65	17.4
E	4.57	1.15	0.46	19.8

[a]See Fig. 10 for definition of a_{side} and b_{side}.
[b]Measured with respect to local mean streamwise direction.

Table 3 End-view correlation results

Position	Major axis dimension, a_{end}, mm	Nondimensional structure size, a_{end}/δ_{local}	Eccentricity, $\varepsilon = 1 - (b_{end}/a_{end})$	a_{end}/a_{side}
A	0.90 ± 0.05	0.55 ± 0.03	0.08 ± 0.05	1.27 ± 0.06
B	1.45	0.75	0.02	1.17
C	2.30	0.98	0.01	0.58
D	2.30	0.83	0.00	0.41
E	3.07	0.77	0.00	0.67

mean structure is quite elongated and nearly oriented in the streamwise direction. Mahadevan and Loth[20] also observed that circular eddies would elongate and flatten as they convected downstream in an $M_c = 0.75$ nitrogen/air shear layer. The mean structure appears more circular at position E, perhaps in response to the localized flow acceleration downstream of reattachment. It is difficult to relate the structural characteristics at position E to previous shear layer work since the pressure field in the wake region is highly nonuniform.[1]

A closer examination of the contour levels at position C reveals that they are not uniformly aligned along a common axis, as was seen at positions A and B. This contour rotation is also quite prevalent at reattachment (position D), where the orientation of the 0.5 contour level and the 0.9 contour level differ by nearly 27 deg. The central correlation contours, i.e., 0.7–0.9, do, however, remain nearly consistent in their inclination for positions A–D. This would suggest that the cores of the large-scale structures are immune from the effects of pressure gradients and other localized influences but that the periphery of the structures is comparatively more susceptible. It would therefore appear that the recompression and reattachment processes are detrimental to the structures' spatial coherency.

Table 2 presents the fundamental statistics describing the correlation fields of Fig. 10. Note that the streamwise evolution of the structures is clearly characterized by a flattening (increased eccentricity) and tilting toward the local streamwise direction (reduced structure angle), except at position E in the wake where the mean structures appear less eccentric with a slightly larger structure angle. A comparison of the present results with the eccentricity data reported by Messersmith[4] (passive scalar method only) and Mahadevan and Loth[20] shows no discernible trend of eccentricity with convective Mach number. Normalization of the structural dimensions by the local shear layer width illustrates that these elongated, tilted mean structures are capable of possessing a spatial extent greater than the local shear layer width; see the a_{side}/δ_{local} column in Table 2.

Messersmith[4] found that decreasing structure angles correlated with increasing convective Mach numbers. However, the structure angles in the present study are clearly seen to decrease from separation through reattachment, despite the nearly constant M_c environment of the shear layer. Tilting of the mean structures is therefore most likely a characteristic of the structures' evolution as they negotiate shear layer formation and compression in the near-wake region. This hypothesis is supported by the cross-correlation measurements of Shau et al.[25] in an $M_c = 0.28$ shear layer. In these experiments, the structures that encountered a shock interaction exhibited a decrease in structure angle. In the present study, the adverse pressure gradient leading up to reattachment mimics the compressive influence of a shock interaction, except that the adverse pressure gradient is less severe and distributed over a greater distance.

The spatial correlation analysis of two supersonic mixing layers ($M_c = 0.51$ and 0.86) by Elliott et al.[3] suggests that the computed shape and orientation of the large-scale structures are dependent upon the transverse location of the reference point within the shear layer. This finding is also reflected in the studies of Shau et al.,[25] who found that the transverse spacing of their pitot probes in an $M_c = 0.28$ shear layer affected the computed structure angle. However, in the present study, no significant variation in the structure shape or angle was observed when the correlation fields were computed using a single transverse reference point that was traversed across the shear layer. This is probably an indication of the highly compressible conditions in the present shear layer ($M_c = 1.3$). The structures in this supersonic convective Mach number regime lack sufficient coherence to maintain a transverse profile of spatial characteristics across the shear layer.

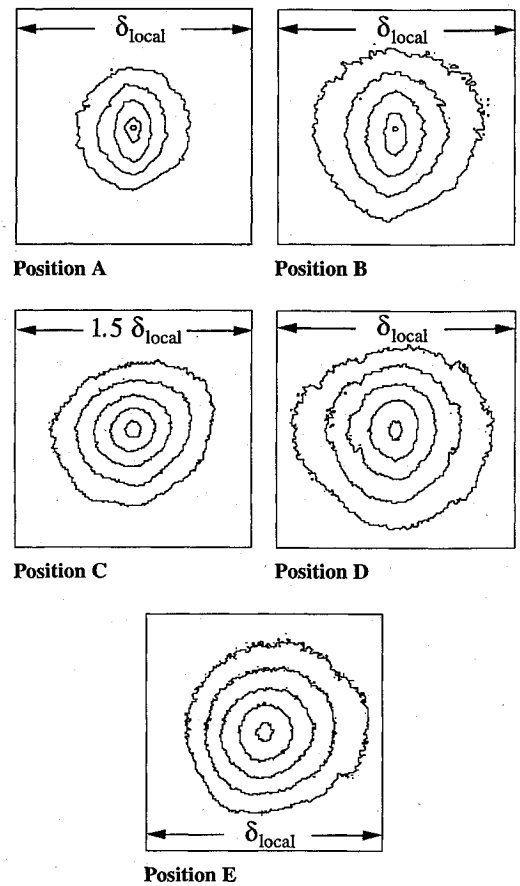

Fig. 11 End-view spatial correlation fields; the contours are in intervals of 0.1 and the outermost contour represents the 0.5 level.

End-View Spatial Correlations

Figure 11 presents the end-view spatial correlation fields. The correlation fields are qualitatively similar at each of the streamwise stations studied, differing appreciably only in their sizes. Table 3 contains the relevant statistical results. As expected, the spanwise symmetry of the correlation fields confirms that the mean flowfield is nominally two dimensional. Accordingly, no angular inclinations are included in Table 3. The contours at positions A and B exhibit a small amount of eccentricity; however, positions C, D, and E are all nearly circular. The nondimensional structure size, a_{end}/δ_{local}, is observed to be an appreciable fraction of the local shear layer width but does not exceed unity.

A comparison of the structure sizes obtained from the side views and end views (presented in the last column of Table 3) shows that at the early stations of the shear layer the mean structures possess a larger correlation distance in the spanwise direction than in the streamwise direction. This would suggest that the initial formation of the shear layer exhibits a slightly preferential organization in the spanwise direction. One possible explanation is that

the rapid expansion at the base corner has effectively filtered the instability modes, thereby retarding the onset of complete three-dimensionality.[26–28] Near recompression, a crossover occurs in the spanwise and streamwise correlation distances, as evidenced by a greater coherency in the streamwise direction than in the spanwise direction for the later streamwise stations C, D, and E.

Conclusions

Pulsed Mie scattering experiments have been performed in an effort to characterize the structural features and spatial evolution of large-scale coherent structures in a planar supersonic base flow. The instantaneous images confirm that coherent motions are active in the separated shear layers and that they exhibit a highly strained organization. The dominant geometrical shape of the structures is elliptical, with the major axis inclined toward the local streamwise direction. The structures are evident at the earliest streamwise station studied and appear to grow without a significant change in eccentricity or structural angle in the zero pressure gradient portion of the shear layer. The organized motions observed in the initial region of the free shear layer are qualitatively similar to previous studies of coherent structures in supersonic mixing layers. The behavior of the shear layer departs from the traditional mixing layer paradigm near recompression, where streamline curvature and an adverse pressure gradient are present. The structures negotiating recompression become a dominant feature of the instantaneous flowfield but begin to lose some of their coherency, especially away from their cores. Furthermore, shocks are seen to emanate from eddies near recompression. The causal relationship between the shock generation and the eddy presence is not clear. The end views contain evidence of large vertical projections that encroach on the interface between the high-speed outer flow and the low-speed recirculation region fluid. The side views and end views of the shear layers illustrate several large-scale entrainment mechanisms.

Spatial statistics computed over a large ensemble of side-view images indicate that the structures evolve during the recompression and reattachment processes by becoming more elliptical and more inclined toward the local streamwise direction. Examination of spatial correlation fields suggests that the cores of these structures remain intact throughout the near-wake region; however, the edges of the coherent structures are degraded by localized flowfield dynamics, such as the adverse pressure gradient of the recompression region. Comparisons of streamwise and spanwise correlation lengths confirm the strong three-dimensionality of the large-scale structures.

Acknowledgments

The authors gratefully acknowledge the financial support of the U.S. Army Research Office, Contract DAAL03-92-G-0129, with Thomas L. Doligalski serving as contract monitor.

References

[1]Amatucci, V. A., "An Experimental Investigation of the Two-Stream, Supersonic, Near-Wake Flowfield Behind a Finite-Thickness Base," Ph.D. Thesis, Dept. of Mechanical and Industrial Engineering, Univ. of Illinois at Urbana–Champaign, IL, 1990.

[2]Clemens, N. T., and Mungal, M. G., "Large-Scale Structure and Entrainment in the Supersonic Mixing Layer," *Journal of Fluid Mechanics*, Vol. 284, 1995, pp. 171–216.

[3]Elliott, G. S., Samimy, M., and Arnette, S. A., "The Characteristics and Evolution of Large-Scale Structures in Compressible Mixing Layers," *Physics of Fluids*, Vol. 7, No. 4, 1995, pp. 864–876.

[4]Messersmith, N. L., "An Experimental Investigation of Organized Structure and Mixing in Compressible Turbulent Free Shear Layers," Ph.D. Thesis, Dept. of Mechanical and Industrial Engineering, Univ. of Illinois at Urbana–Champaign, IL, 1992.

[5]Ragab, S. A., and Wu, J. L., "Linear Instabilities in Two-Dimensional Compressible Mixing Layers," *Physics of Fluids A*, Vol. 1, No. 6, 1989, pp. 957–966.

[6]Sandham, N. D., and Reynolds, W. C., "Compressible Mixing Layer: Linear Theory and Direct Simulation," *AIAA Journal*, Vol. 28, No. 4, 1990, pp. 618–624.

[7]Sandham, N. D., and Reynolds, W. C., "Three-Dimensional Simulations of Large Eddies in the Compressible Mixing Layer," *Journal of Fluid Mechanics*, Vol. 224, 1991, pp. 133–158.

[8]Samimy, M., and Addy, A. L., "Interaction Between Two Compressible, Turbulent Free Shear Layers," *AIAA Journal*, Vol. 24, No. 12, 1986, pp. 1918–1923.

[9]Amatucci, V. A., Dutton, J. C., Kuntz, D. W., and Addy, A. L., "Two-Stream, Supersonic, Wake Flowfield Behind a Thick Base, Part 1: General Features," *AIAA Journal*, Vol. 30, No. 8, 1992, pp. 2039–2046.

[10]Clemens, N. T., and Mungal, M. G., "A Planar Mie Scattering Technique for Visualizing Supersonic Mixing Flows," *Experiments in Fluids*, Vol. 11, No. 2/3, 1991, pp. 175–185.

[11]Clumpner, J. A., "Light Scattering from Ethyl Alcohol Droplets Formed by Homogeneous Nucleation," *Journal of Chemical Physics*, Vol. 55, No. 10, 1971, pp. 5042–5045.

[12]Samimy, M., and Lele, S. K., "Motion of Particles with Inertia in a Compressible Free Shear Layer," *Physics of Fluids A*, Vol. 3, No. 8, 1991, pp. 1915–1923.

[13]Kline, S. J., and McClintock, F. A., "Describing Uncertainties in Single-Sample Experiments," *Mechanical Engineering*, Vol. 75, No. 1, 1953, pp. 3–8.

[14]Bogdanoff, D. W., "Compressibility Effects in Turbulent Shear Layers," *AIAA Journal*, Vol. 21, No. 6, 1983, pp. 926, 927.

[15]Papamoschou, D., and Roshko, A., "The Compressible Turbulent Shear Layer: An Experimental Study," *Journal of Fluid Mechanics*, Vol. 197, 1988, pp. 453–477.

[16]Monaghan, M. A., "Tests of Humidity Effects on Flow in a Wind Tunnel at Mach Numbers Between 2.48 and 4.00," Aeronautical Research Council, Current Paper 247, London, 1956.

[17]Paul, P. H., van Cruyningen, I., Hanson, R. K., and Kychakoff, G., "High Resolution Digital Flowfield Imaging of Jets," *Experiments in Fluids*, Vol. 9, No. 5, 1990, pp. 241–251.

[18]Goebel, S. G., and Dutton, J. C., "Experimental Study of Compressible Turbulent Mixing Layers," *AIAA Journal*, Vol. 29, No. 4, 1991, pp. 538–546.

[19]Brown, G. L., and Roshko, A., "On Density Effects and Large Structure in Turbulent Mixing Layers," *Journal of Fluid Mechanics*, Vol. 64, Pt. 4, 1974, pp. 775–816.

[20]Mahadevan, R., and Loth, E., "High-Speed Cinematography of Compressible Mixing Layers," *Experiments in Fluids*, Vol. 17, No. 3, 1994, pp. 179–189.

[21]Elliott, G. S., Samimy, M., and Arnette, S. A., "Study of Compressible Mixing Layers Using Filtered Rayleigh Scattering Based Visualizations," *AIAA Journal*, Vol. 30, No. 10, 1992, pp. 2567–2569.

[22]Dimotakis, P. E., "On the Convection Velocity of Turbulent Structures in Supersonic Shear Layers," AIAA Paper 91-1724, 1991.

[23]Clemens, N. T., and Mungal, M. G., "Two- and Three-Dimensional Effects in the Supersonic Mixing Layer," *AIAA Journal*, Vol. 30, No. 4, 1992, pp. 973–981.

[24]Miles, R., and Lempert, W., "Two-Dimensional Measurement of Density, Velocity, and Temperature in Turbulent High-Speed Air Flows by UV Rayleigh Scattering," *Applied Physics B: Photo-Physics and Laser Chemistry*, Vol. 51, No. 1, 1990, pp. 1–7.

[25]Shau, Y. R., Dolling, D. S., and Choi, K. Y., "Organized Structure in a Compressible Turbulent Shear Layer," *AIAA Journal*, Vol. 31, No. 8, 1993, pp. 1398–1405.

[26]Herrin, J. L., and Dutton, J. C., "Effect of a Rapid Expansion on the Development of Compressible Free Shear Layers," *Physics of Fluids*, Vol. 7, No. 1, 1995, pp. 159–171.

[27]Dussauge, J. P., and Gaviglio, J., "The Rapid Expansion of a Supersonic Turbulent Flow: Role of Bulk Dilatation," *Journal of Fluid Mechanics*, Vol. 174, 1987, pp. 81–112.

[28]Narasimha, R., and Viswanath, P. R., "Reverse Transition at an Expansion Corner in Supersonic Flow," *AIAA Journal*, Vol. 13, No. 5, 1975, pp. 693–695.